Receptivity of the BoLT-II Boundary Layer to Freestream Disturbances and Surface Roughness

Zachary M. Johnston, Luke J. Melander and Graham V. Candler
University of Minnesota
Minneapolis, MN, USA.

February 1, 2022

Abstract: Current work seeks to investigate the non-modal growth effects induced by the nosetip of the Boundary Layer Turbulence (BoLT-II) configuration. Flow decomposition methods will be applied to datasets obtained from high-fidelity computations in order to understanding the relevant transition mechanisms for flight. The low noise environment of quiet wind tunnels provides a reasonable representation of flight environments up to a particular range of Reynolds number conditions before wind tunnel noise can significantly contribute to early transition. However, the Reynolds numbers are much higher in flight where subscale experimental campaigns may be insufficient to maintain the low-level noise environment that is representative of flight conditions for hypersonic vehicle design. Therefore, this work will reveal the dominant transition mechanisms contributing to the transition process on BoLT-II. Direct Numerical Simulation (DNS) will be performed to compare non-modal growth effects at subscale wind tunnel conditions and full scale flight conditions using US3D.

Keywords: Hypersonic Flow, Boundary Layer Transition, Computational Fluid Dynamics, BOLT-II.

1 Introduction

Understanding transition mechanisms in hypervelocity boundary layers is important for predictive design and control of aerospace vehicles. This is due to the fact that laminar-turbulent transition of boundary layer flows have a direct impact on surface skin friction and aerodynamic heating affecting hypersonic vehicle performance. Transition studies for canonical flow problems (i.e. cones, flat plates, or wedges) have provided fundamental understanding but at the expense of using analysis tools that do not scale well when applied to realistic flight geometries or flow conditions. To address some of the unsolved problems, the BoLT-II hypersonic flight experiment is meant to collect flight data to help verify and develop the tools for boundary layer transition and turbulence studies [1]. The effect of the nosetip on the transition process on BoLT-II has not been extensively studied. Non-modal growth of roughness along the nosetip could trip early transition, and the high curvature of the bow shock could be a source of vorticity that interacts with downstream instabilities. These mechanisms may be dominant at higher Reynolds numbers as seen in flight but not at the conditions used in the subscale wind tunnel tests. This is important since ground test campaigns are heavily used to dictate vehicle design but are restricted

to flow regimes where the flow is expected to remain linear or at most transitional. Higher Reynolds number conditions can be achieved in wind tunnels to observe turbulent heating but at the cost of unrealistic acoustic noise levels that are not representative of flight. In this work, we investigate the effect of the nosetip of BoLT-II on the transition process using forced low dissipation direct numerical simulation.

2 Problem Statement

The three-dimensional flow features produced by the BoLT shape are shown in Fig. 1 at $Re/m = 10.3\text{x}10^6$. The nose of the geometry is a two-dimensional cylindrical leading edge that is revolved to four swept edges and joined by concave surfaces in the azimuthal direction. The hypersonic flow around the surface curvature produces a bow shock with high curvature. It is postulated that a shock-shock interaction is a source of vorticity post-shock. Therefore, one of the goals of the current work is to quantify the disturbance amplification inherent to the shock structure at hypersonic conditions.

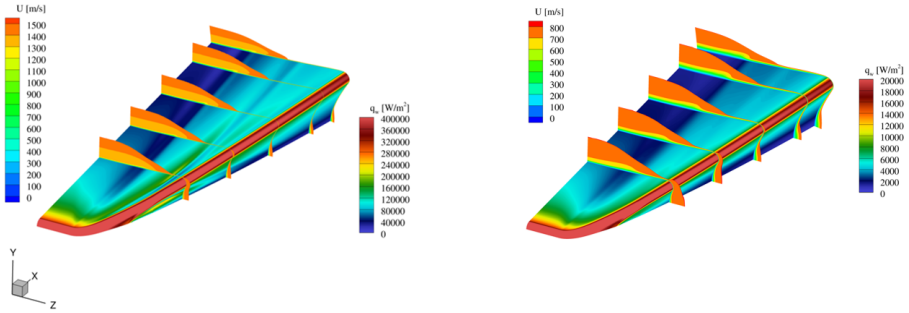

Figure 1: Steady state flowfields of flight (left) and subscale (right) configurations.

Recent work has shown that a dominant flow response for blunted cone configurations appears in the form of low-frequency steady streamwise structures, set off by freestream noise and surface roughness [4]. The dominance of this response scales with Reynolds number and bluntness. This non-modal growth mechanism likely exists on the blunted leading edge of the BoLT-II geometry, and could be a dominant response at the high Reynolds numbers expected in flight. Therefore, a comparison between the flight and the subscale configurations will be used to investigate the dominance of this mechanism.

3 Computational Methodology

3.1 Numerical Method

The three-dimensional compressible Navier-Stokes equations are solved using the unstructured finite volume code, US3D, developed at the University of Minnesota [2]. The code and numerical method have been extensively tested and validated for a variety of unsteady compressible flow problems.

$$\frac{\partial \mathbf{U}}{\partial t} + \frac{\partial}{\partial x_i}\left(\mathbf{F}_i^c - \mathbf{F}_i^v\right) = 0 \tag{1}$$

The state vector is represented by $\mathbf{U} = [\rho, \rho u_i, E]^T$ and the components of the flux vector, $\mathbf{F}$, are represented by the convective flux, $\mathbf{F}_i^c = [\rho u_i, \rho u_i u_j + \delta_{ij} p, (E+p)u_i]^T$, and the diffusive flux, $\mathbf{F}_i^v = [0, \mathbb{T}_{ij}, u_i \mathbb{T}_{ij} - q_i]^T$.

A version of the kinetic energy consistent (KEC) flux evaluation scheme [3] is used along with implicit time integration allowing us to compute converged solutions within a reasonable amount of time. The low dissipation KEC inviscid fluxes are computed as a sum of a non-dissipative, central, fourth-order scheme and a dissipative portion of the modified Steger-Warming shock capturing scheme. The non-dissipative central component is used for the primary flux evaluation and we apply a small portion of the dissipative component taking the following form,

$$\boldsymbol{F} = \boldsymbol{F}_{central} + \alpha \boldsymbol{F}_{diss}. \tag{2}$$

The dissipation portion is tailored using a shock detection switch, α, which is a combination of a switch similar to Larsson et al. [5] along with a filtering step based on velocity divergence (dilatation). Simply using a dilatation cutoff introduces an unwanted amount of dissipation in the boundary layer near the nosetip. Therefore, the filtering step allows us to tune the dissipation factor to the shock and ensures the dissipation factor remains constant in time. The base shock sensor takes the following form:

$$D_f = -\partial_j u_j / (1.5\sqrt{\omega_j \omega_j} + 0.05c/h) \tag{3}$$

c is the local speed of sound and h is a normalized length that is taken as the cube root of the cell volume that is locally evaluated. The shock-capturing scheme is activated primarily at discontinuities (i.e. shocks) by adding dissipation in regions where compression is high. When using equation (3) to compute the dissipation without the filtering step, a slightly higher amount of dissipation is applied near the shock and at the stagnation plane than what is desired. Therefore, by filtering the dissipation field computed from equation (3), we can sharpen the dissipation factor near the shock and ensure smoothly varying values.

The introduced shock sensor is filtered by the divergence of velocity, similar to Hendrickson et al. [6], taking the following form:

$$\beta = \frac{(\nabla \cdot \mathbf{u})^2}{(\nabla \cdot \mathbf{u})^2 + \left(\nu \frac{|\mathbf{u}|}{h}\right)^2 + \epsilon} \tag{4}$$

ν is the tuning parameter and is set to 0.005. ϵ is a very small value to avoid divide by zero. By using the base shock sensor from equation (3) and the dilatation filter from equation (4) we obtain the tuned sensor:

$$\alpha = [\max((D_f - \phi), 0)]\, \beta + \phi \tag{5}$$

ϕ is a user defined parameter that sets the minimum dissipation factor globally. For the current computations, ϕ is set to 0.01 in order to maintain numerical stability.

3.2 Grid Resolution

A grid with minimal stretching and skewness is needed for stability and accuracy with the low-dissipation numerical method. Designing the grid in this way allows for a smoothly varying grid spacing and approximately orthogonal cell structures at critical regions in the flowfield (i.e. at the bow shock). The grids in this work have improved grid alignment with the shock curvature. This is very important when passing disturbances through shocks since large variations in grid spacing and poor shock alignment can produce a significant amount of error.

For simulating boundary layer instabilities, it is important that the grid has a sufficient resolution to resolve relevant wavenumber (frequency) content. Additionally, the grid needs to respect the wave damping characteristics of the numerical method used in the external forcing

simulations. Therefore, testcases were performed on a one-dimensional domain using planar wave propagation with a dissipation factor of 0.01 to ensure the current grid properly resolves a 600kHz wave propagating the length of the domain (1 meter) in the streamwise direction at flight conditions. This was chosen based off the highest N-factors for second-Mack mode disturbances at close to the same flight conditions from NPSE analysis performed by Texas A&M University. The current grid that encompasses the entire flight configuration contains 580 million elements for the full-scale, 1 meter length geometry.

In order to focus on the analysis of the nose portion, the same grid is truncated to approximately 25% of the domain length resulting in a subdomain with 135 million total elements. Therefore, separate simulations will be performed on the nosetip subdomains and is where the majority of the analysis will be carried out. This reduces the computational cost of the computations while maintaining a consistent grid resolution. Preliminary steady-state solutions are shown in Fig. 1.

3.3 Unsteady Forcing: Freestream Disturbances

Before introducing disturbances, a steady-steady solution is fully converged and is defined as the baseflow state in this work. After the baseflow state is obtained, small amplitude disturbances in the primitive variables are introduced using a sustained, broadband stochastic forcing approach. The fluctuations in the primitive variables are a function of a random number, $r_i \epsilon [-1, 1]$, obtained with the FORTRAN pseudo-random number generator that is computed at each timestep. The amplitude, A, is non-dimensionalized and scaled based off the Chu [7] energy norm so that the disturbance energy is very low relative to the total freestream energy. The disturbance forcing approach is shown below.

$$(u_r, v_r, w_r, T_r, \rho_r) = r_i \epsilon (-1, 1)$$
$$E_d = \left[{u_r}^2 + {v_r}^2 + {w_r}^2 + {T_r}^2 \frac{1}{\gamma(\gamma-1){M_\infty}^2} + {\rho_r}^2 \frac{1}{\gamma {M_\infty}^2} \right]^{\frac{1}{2}} \tag{6}$$

$$(u', v', w', T', \rho') = A(u_r, v_r, w_r, t_r, \rho_r) \frac{1}{E_d} diag(|\vec{U}|, |\vec{U}|, |\vec{U}|, \bar{T}, \bar{\rho}) \tag{7}$$
$$p' = (\rho' \bar{T} + T' \bar{\rho}) R_{air}$$

3.4 Steady Forcing: Wall Roughness

In order to generate surface roughness, we utilize a random disturbance function to investigate the effects of roughness. Each wall node is perturbed using a random number, between (-1,1), multiplied by a maximum amplitude. The displacement is smoothed along grid connected lines, similar to the approach used by Dinzl & Candler [8]. Previous work by Thome et al. [9] showed that different heating patterns are observed on the BoLT configuration using different roughness wavenumber distributions. However, a non-biased wavenumber distribution allows for an exploratory look at the flowfield response without filtering out potentially relevant disturbances. Additionally, spectral proper orthogonal decomposition extracts the resolvent modes if the flowfield forcing is stochastic and the sampled flowfield is statistically steady.

3.5 Spectral Proper Orthogonal Decomposition Analysis

In the current work we will utilize the spectral proper orthogonal decomposition (SPOD). This approach approximates the two-point space-time correlation (covariance) tensor associated with

the flow response [10],

$$\mathbf{C}(x, x', t,' t) = \mathbb{E}\left(q(x,t)q(x',t)\right) \tag{8}$$

$\mathbb{E}$ is the expectation operator and $q(x,t)$ is the state of interest. For stationary states, an efficient implementation can be derived in the frequency domain by expanding the Fourier modes [11],

$$\hat{q}(x,f) = \sum_{j=1}^{\infty} a_j(f)\psi_j(x,f) \tag{9}$$

where f is the temporal frequency and expansion coefficients are $a_j(f) = \langle \hat{q}(x,f), \psi_j(x,f) \rangle$ with an appropriate definition of the inner product $\langle \cdot, \cdot \rangle$ in the spatial domain. We define the inner product in this work with Chu's disturbance energy norm.

Stationary two-dimensional snapshots are taken of the flowfield and are equally spaced in time. If the flow is forced stochastically and is at a statistical steady-state, each snapshot is considered a separate run, and the resulting SPOD modes are the resolvent modes. Flowfield structures and the energy gain associated with them can then be studied.

4 Future Work

Direct numerical simulation will be used to simulate the steady and unsteady flowfields using US3D with the numerical scheme described previously. The unsteady simulations will include stochastic freestream forcing of the baseflow solution as well as surfaces roughness. The freestream forcing will be achieved using an external forcing function that will introduce disturbances in the freestream that pass through the shock. This will allow us to observe the dominant flow response due to the bow shock curvature. Furthermore, surface roughness will be imposed onto the geometry to increase the receptivity of the structures [4]. Boundary layer modes will be identified using SPOD and ranked by their energy gain. This will reveal the modes that are most likely to contribute to transition. Additional analysis on the domain extending the full length of the BoLT-II geometry will be performed. This is intended to quantify how the disturbances of the receptivity process may contribute to the later stages of the transition process at flight conditions where the boundary layer is likely to be in a transitional state.

References

[1] Johnston, Z. M., Hemati M. S., and Candler, G. V. "Modal Analysis of Instabilities in the BoLT-2 Flowfield," AIAA 2022-0348.

[2] Candler, G. V., Barhhardt, M. D., Drayna T. W., Nompelis,I., Peterson, D. M., and Subbareddy, P. K. "Unstructured grid approaches for accurate aeroheating simulations," AIAA Paper, Vol. 3959, 2007.

[3] Subbareddy, P. K. and Candler, G. V. "A fully discrete, kinetic energy consistent finite-volume scheme for compressible flows," *Journal of Computational Physics*, Vol. 228, No. 5, 2009, pp. 1347-1364.

[4] Melander, L. J., Dwivedi, A., and Candler,G. V. "Nose Bluntness Effects on the Amplification of External Disturbances in Hypersonic Flows," AIAA 2022-0948.

[5] Larsson, J., Vicquelin, R., and Bermejo-Moreno I. "Large eddy simulations of the HyShot II scramjet," *Center of Turbulence Research Annual Research Briefs*, 2012, pp. 241-251.

[6] Hendrickson, T., Kartha, A., and Candler, G. V. "An Improved Ducros Sensor for the Simulation of Compressible Flows with Shocks," AIAA 2018-3710.

[7] Chu. B. T. "On the energy transfer to small disturbances in fluid flow (Part I)," *Acta Mechanica*, Vol. 1, No. 3, 1965, pp. 215-234]

[8] Dinzl, D. J. and Candler, G. V. "Direct simulation of hypersonic crossflow instability on an elliptic cone," *AIAA Journal*, Vol. 55, No. 6, 2017, pp. 1769-1782.

[9] Thome, J. S., Reinert, J. D., and Candler, G. V. "Effect of steady forcing on BoLT flowfield for flight Reynolds Numbers," AIAA 2020-1042.

[10] Lumley, J. L. "Stochastic tools in turbulence," Courier Corporation, 2007.

[11] Towne, A., Schmidt, O. T., and Colonius, T. "Spectral proper orthogonal decomposition and its relationship to dynamic mode decomposition and resolvent analysis," *J. Fluid Mech.*, Vol. 847, 2018, pp. 821-867.